Contents lists available at NCBI

The American Journal of Science and Medical Research

Journal homepage: http://ajsmrjournal.com/

Research Article

Potential usage of Zerumbone to suppress inflammation: An *in silico* study

Muhammed Amanat[1]*, A F M Shahid Ud Daula[2], Fakhrul Islam[2]

[1]*Department of Pharmacology, Central University of Punjab, Ghudda, Bathinda, Punjab-151401, India*
[2]*Department of Pharmacy, Noakhali Science and Technology University, Sonapur, Noakhali-3814, Bangladesh*

*Corresponding author:
E-mail:
amanat.pharmacy@easternuni.edu.bd

Keywords: Zerumbone, Inflammation, Docking, QSAR, ADMET, MD Simulation

https://dx.doi.org/10.5281/zenodo.7215994
Received: 2 April 2022;
Accepted: 22 May 2022;
Published: 4 June 2022

ABSTRACT

A significant cyclic sesquiterpenoid known as Zerumbone was extracted from *Zingiber roseum* using the volume liquid chromatographic (VLC) technique. It's a naturally occurring phytochemical having a variety of physiological properties, including antioxidant, anti-ulcer, and antiproliferative action. This study's major goal was to evaluate Zerumbone's anti-inflammatory effectiveness against the inflammation receptors-Secretory Phospholipase A2 (sPLA2), Cyclooxygenase-2 (COX-2), Tumor Necrosis Factor (TNF-alpha), and Inducible Nitric Oxide Synthase 4 using various in-silico methods. The targeted receptors were obtained from Protein Data Bank, and the ligand was accessed in the Pubchem database. Utilizing the Autodock PyRx platform, which supports Autodock Vina, molecular docking was carried out. Even in the computational prediction, it was revealed that this substance was non-toxic. Receptors exhibiting the highest binding affinity for our ligand were further investigated using molecular dynamics (MD) simulations with WebGRO, CABS-flex, and iMODS web servers. The molecular docking outcomes showed that our ligand molecule exhibited the highest binding affinity for the sPLA2 receptor. MD simulation studies also showed good leads to sPLA2. In conclusion, our outcomes suggest that Zerumbone is an important inhibitor of sPLA2 and might be further utilized as a potential anti-inflammatory agent.

1. Introduction

It's hard to misjudge the significance of plant life to human beings. There has been a significant increase in public interest in medicinal plants. In a variety of traditional remedies all over the world, herbs are needed to treat various ailments [1, 2]. Discovering medicines, extracted from natural plants is not always hard; they are also affordable, non-toxic, and potent. In addition, they no longer cause many side effects [3]. Medicinal plants remain the world's most important source of medications, just behind the "World Health Organization" (WHO). In developed countries, 80 percent of people use conventional remedies made from medicinal herbs [4] and showed several pharmacological activities similar to anticancer [5], antimicrobial [6], anti-inflammatory activities [7], etc.

Today, numerous people around the world suffer from inflammatory diseases. Our bodies secrete inflammatory mediators uncontrollably when we have inflammatory disorders. Inflammation aids the body as resistance against injury or pathogens. Through inflammation, the cell produces and discharges some proinflammatory cytokines that cause many important cellular effects including heart problems, asthma, rheumatoid arthritis, type 2 diabetes, and malignance [8-10].

Extracellular enzymes known as Secretory Phospholipases A2 (sPLA2s) play a significant role in inflammation. There are nine different members of the human phospholipase A2 family, each with its own tissue distribution, hydrolytic activity, and phospholipid substrate specificity [11]. Human inflammatory cells express sPLA2s isoforms as neutrophils, eosinophils, and basophils. Arachidonic acid, the first substrate for an aggregate of pro-inflammatory eicosanoids that cause inflammation, is released from specific sPLA2 [12-14]. These enzymes modulate cellular processes, eliminate bacteria directly, or influence inflammatory responses through lipase activity. Selective sPLA2 receptor antagonists are also effective for controlling autoimmune diseases and allergic conditions such as rheumatoid arthritis and respiratory disease [12].

When stimulated by phospholipase A2, membrane phospholipids secrete arachidonic acid, a precursor of the cyclooxygenase (COX) enzyme [15, 16]. This enzyme is in

charge of producing the crucial inflammatory mediator prostaglandin [17, 18]. In general, three different COX enzyme types are found, namely COX1, COX2, and COX3, and each of them has unique pharmacological properties. However, the inducible COX2 enzyme is found at the place of inflammatory regions [19-22]. By inhibiting this COX2 enzyme, inflammatory and painful sensations are diminished [19].

Tumor necrosis factor (TNF) is a potent cytokine with multiple pharmacological activities. TNF induces necrosis and apoptosis of tumor cells [23] and is a major mediator of acute and chronic systemic inflammatory responses [24]. TNF is not only self-secreted but also stimulates the assembly of other inflammatory cytokines. Correspondingly, it plays a major role in chemotherapy-induced septic shock in patients with advanced carcinoma [25]. Furthermore, it plays a significant role in autoimmune illnesses such as rheumatoid arthritis (RA), inflammatory bowel diseases, ulcerative colitis and sclerosis [23]. Thus, TNF inhibition alleviates inflammation and pain.

Nitric oxide (NO) is secreted through the action of Nitric Oxide Synthase (NOS) enzymes from L-arginine in a mammalian cell [19]. NOS isoenzymes are subdivided into nNOS (constitutive in neuronal tissue), eNOS (constitutive in vascular endothelial cells), and iNOS (inducible by cytokine in macrophages and hepatocytes) [26]. A small quantity of NO is produced via nNOS and eNOS, in which higher quantities of NO are constructed from iNOS. A few microbial products, including lipopolysaccharide (LPS) and anti-inflammatory cytokines, have an effect on iNOS [27]. These NO secretion is improved in response to inflammatory provocations and arbitrates the unfavorable conditions [28] e.g., sepsis, septic shock, vascular dysfunction in diabetes, asthma, arthritis, multiple sclerosis, and inflammatory diseases of the gut [29]. Molecules inhibiting the activity of iNOS are recommended to be potential anti-inflammatory drugs.

NSAIDs, typically mentioned as non-steroidal anti-inflammatory medicine, are typically utilized in combination with internal secretion treatments to treat inflammatory reactions. Though these preparations have potent anti-inflammatory effects, long-term use of them contains a range of adverse consequences, as well as damage to the GI tract. Several initiatives are created in recent years to form medicines that do not solely have glorious anti-inflammatory efficiency however even a few adverse effects have. The event of contemporary prescribed drugs has long used natural ingredients [30]. There is evidence that drugs made from natural ingredients affect the activity of second messengers such as cGMP, cAMP, protein kinases and calcium, inflammatory molecules, such as inducers of NO synthase (iNOS), cyclooxygenase (COX2), and other inflammatory mediators. [31-33].

The primary bioactive component in the rhizome of *Zingiber roseum* (Family: Zingiberaceae) is Zerumbone, a naturally occurring cyclic sesquiterpene [34]. It was isolated from the rhizomes of *Zingiber roseum* by vacuum liquid chromatography (VLC) [34]. In the Gazipur and Tangail districts of Bangladesh, traditional healers use the rhizome of *Zingiber roseum* to treat rheumatism, asthma, and stomach ulcers and wounds. Due to its natural composition, it has an extensive array of pharmacological activities including antioxidant, anti-inflammatory, anti-proliferative, and antiulcer activities [35-38]. Zerumbon has many therapeutic benefits, making it one of the compounds in demand in the field of drug discovery. Data from in vivo tests show that Zerumbone has an anti-inflammatory impact [39, 40]. Calculating the anti-inflammatory potentials was the investigation's main goal of previously synthesized Zerumbone using various in-silico methods. Several inflammatory receptors, including Secretory Phospholipase A2, Cyclooxygenase-2, Tumor Necrosis Factor, and Inducible Nitric Oxide Synthase, were docked with the chosen molecule in this investigation [10]. Moreover, QSAR, ADMET, Bioactivity and Toxicity Score analysis, and molecular dynamics modeling were used to assess drug likelihood properties and ligand-receptor stability.

2. Materials and Methods

2.1 PASS Computer Program

PASS is a computer-based instrument that predicts various forms of functional activity for a wide range of ingredients that contain phytoconstituents. The estimated activity of chemical substances is forecasted as probable activity (Pa) and probable inactivity (Pi). Only molecules with a Pa larger than Pi are assumed to be suitable for particular therapeutic procedure [41-43].

2.2 *In silico* study

2.2.1 Ligand preparation and optimization

Following Gasteiger's method, the net charge of the molecule was adjusted to "zero," the indicated ligand Zerumbone (Figure 1) was obtained from the PubChem database as part of the optimization based on "UCSF Chimera Software Version-1.14" [44]. All preferred molecules were transformed to mol2 format after minimizing energy, a crucial factor of the molecular docking strategy [45].

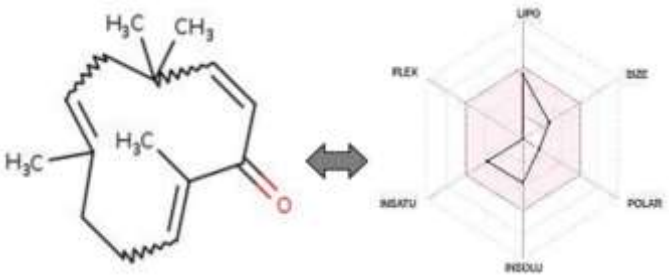

Figure 1. 2D Structure of ligand Zerumbone and its pharmacokinetic sign

2.3 Protein Preparation

The non-mutated, tertiary micro-crystal structures of the targeted receptors Secretory Phospholipase A2 (PDB-ID: 4UY1), Cyclooxygenase-2 (PDB-ID: 5IKT), Interleukin-1 Receptor-associated Kinase 4 (PDB-ID: 5KX7), Tumor Necrosis Factor (PDB-ID: 2AZ5) and Inducible Nitric Oxide Synthase 4 (PDB-ID: 4NOS) were retrieved from the Protein Data Bank [10, 46], as the receptor macromolecule of the research (Figure 2). Proteins have been consistently optimized in terms of protein chain selection by removing undesirable objects such as heteroatoms, ligands, water fragments, metal ions, and extra chain components that interfere with receptors. Moreover, protein optimization for ideal docking also include addition of the required hydrogen atoms. The program "UCSF Chimera Software Version-1.14" [45], was applied to conduct the overall optimization, and the optimized protein assembly was then extracted and conserved for future investigations.

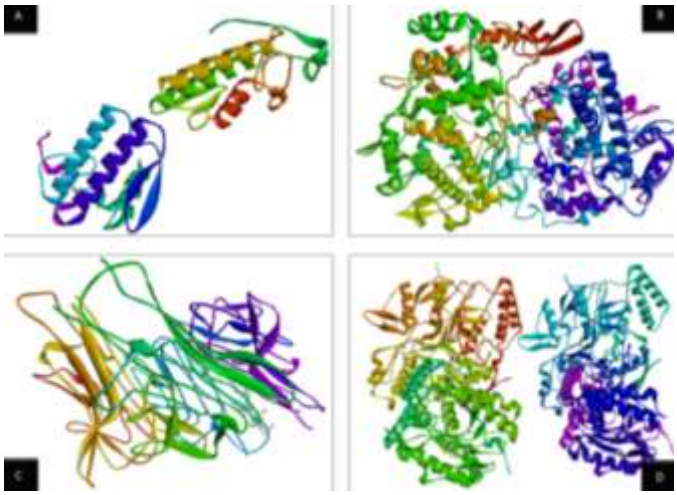

Figure 2. 3D structures of all targeted receptors. A) Secretory Phospholipase A2. B) Cyclooxygenase-2. C) Tumor Necrosis Factor. D) Inducible Nitric Oxide Synthase 4

2.4 Molecular docking

Molecular docking strategies are vital part of natural science as well as the most widely used technique during drug development. The molecular docking investigation was analyzed using the PyRx 0.8 tool (based on the Auto-Dock Vina). In Chain A of each targeted receptor, we employed the blind docking approach for docking [47]. Based on the RMSD readings, AutoDock Vina results were used to compute each complex binding interactions.

2.5 Visualization of the Docked File

After finishing the ligand dockings on the macromolecule separately, the two PDBQT output files from the PyRx program were downloaded. The DS Visualizer was used to view the protein-ligand complex structures (64-bit) [48].

2.6 Molecular dynamics simulation

WebGRO and CABS-flex server v2.0 were used to perform molecular dynamics (MD) simulations of protein-ligand complexes [49, 50]. Two fundamental measures, such as RMSD (root mean square deviation) and RMSF (root mean square fluctuation), were used to assess the stability of complexes. The WebGRO server was used to analyze the RMSD patterns of protein-ligand complexes. Using the GROMOS96 43a1 force-field, the best-docked protein-ligand complexes were constructed for MD. The PRODRG tool [51] was used to build the ligand topology. SPC was chosen as a solvent model for the protein-ligand complex (triclinic water box of 50×75×70 Å) [52]. Based on the overall charges, this system was neutralized by adding sodium or chlorine ions. The steepest descent algorithm (5000 steps) was used to minimize the system before MD. The MD simulations were run with 0.15 M NaCl in the presence of a constant temperature (300 K) and pressure (1.0 bar). The number of frames in each simulation was about 1000, and the simulation time was 100 ns. CABS-flex 2.0 was used to assess the flexibility of the structure (RMSF). CABSflex is an efficient tool for rapidly modeling protein residue flexibility to correlate with protein flexibility data obtained by NMR spectroscopy [53]. The cycle count was set at 50. The cycle count between trajectory frames has been increased to 50. Other settings were left at their default values. The iMODS server was also used to simulate molecular dynamics in this study. The iMODS tool facilitates normal mode analysis by generating accessible information on pathways that may involve macromolecules or homologous structures [10].

2.7 Prediction of *in silico* pharmacokinetic and Physic-chemical properties

2.7.1 ADMET prediction

To ascertain a ligand's role within the body, its ADMET must be considered a pharmacokinetic feature. The use of computerized screening methods to characterize the absorption, distribution, metabolism, excretion, and toxicity (ADMET) of potential molecules significantly increases the chances of drug development and innovation success. These pharmacokinetic scores provide an imaginative view into the activity of target molecules in the body system and anticipate their use as drug targets. Following molecular docking studies, ADMET properties of selected ligands were investigated using preADMET, an online pharmacokinetic property prediction tool [44]. Caco-2 cell permeability, Madin-Darby Canine Kidney (MDCK) cell permeability, skin permeability, plasma protein binding (PPB), human intestinal absorption, blood-brain barrier penetration, and toxicity features such as a mutagenic or irritating impact are examples of physiochemical properties [44]. Penetration through the blood-brain barrier (BBB) is a vital part of the distribution of drug candidates in the central nervous system (CNS). Candidate drugs with optimal ability to cross the BBB are said to be active in the CNS. The BBB penetration coefficient must be greater than 0.40 (> 0.40). In contrast, inactive CNS candidates have a BBB penetration coefficient of less than 0.40 (<0.40). Plasma protein binding (PPB) determines the distribution and availability of unbound compounds in the target site and determines drug efficacy. Strongly bound drug candidates have a plasma protein binding percentage of more than 90% (% PPB > 90%), and weakly bound candidates have less than 90% (% PPB < 90%). In addition, in vitro models of Caco-2 cell permeability and MDCK cell permeability have been successfully used as trustworthy approaches to predict intestinal absorption of oral medicine. Compounds are categorized according to their permeability values in Caco-2 cells as poor, moderate, and high permeability. Compounds with values greater than 70 (cell permeability > 70) are high permeability, values among 4-70 are moderate permeability, and values less than 4 are low permeability across Caco-2 cells. Similarly, MDCK cell permeability values >500 predict a compound as highly permeable, values within 25-500 are reasonably permeable, and values below 25 have low permeability. Correspondingly, research on human intestinal absorption (HIA) and skin permeability can also be used to identify therapeutic candidates that can be taken orally. According to their growing negative value, molecules in an in-silico experiment exhibit features like skin permeability. A percent HIA score of 70 to 100 indicates that the component has strong absorbance. The bioavailability of medications injected into the portal circulation is evaluated by the percentage of human intestinal absorption (% HIA). Because of toxicity, a drug candidate may be disqualified during drug discovery despite having good biological features. A chemical is recommended as a safe medication when an in-silico toxicity outcome is negative. Additionally, using the web-based pkCSM-pharmacokinetics server, the toxicity of the selected bioactive compounds was further assessed [54].

2.7.2 QSAR studies

Using molinspiration cheminformatics software tools, the quantitative structure-activity relationship (QSAR) descriptors

of chosen ligand were investigated [44]. Molinspiration virtual screening engine v2018.10 was used to investigate the parameters. These features were also predicted using the OSIRIS property explorer, a open server for predicting molecular properties [55].

2.7.3 Boiled-Egg analysis

A boiled Egg was employed to predict blood-brain barrier permeability as well as gastrointestinal absorption of our chosen phytochemical Zerumbone. As a result of analyzing the BOILED-Egg graph, the compound in the yellow part of the graph showed high blood-brain barrier permeability, and the compound in the white part of the graph showed higher absorption properties in the gastrointestinal tract. The SwissADME website was used to analyze the BOILED-Egg graphic. [56] . The SwissADME website is a free program that predicts the pharmacokinetics and drug-likeness features of bioactive substances [57-59].

2.7.4 Bioactivity and toxicity risks prediction

Applying molinspiration and the Osiris property explorer, a selection of ligands were assessed for a variety of bioactivities and toxicity risks. Kinase inhibitor (KI), enzyme inhibitor (EI), a protease inhibitor (PI), ion channel modulator (ICM), G protein-coupled receptor ligand (GPCRL), and nuclear receptor-ligand interaction (NRL) were all evaluated for bioactivity. Factors including drug score and drug likeness were used to estimate toxicity risks. The selected ligands were predicted to be non-toxic by the analysis.

3. Results and Discussion

Table.1 Pass online activity of Zerumbone

Name	Main predicted activity	Pass-online activity	
		Pa	Pi
Zerumbone	▪ Anti-inflammatory activity	0.831	0.005
	▪ Apoptosis agonist	0.811	0.007
	▪ Antineoplastic	0.801	0.012
	▪ Antieczematic	0.799	0.019
	▪ Phosphatase inhibitor	0.620	0.038
	▪ Antihelmintic (Nematodes)	0.581	0.008
	▪ Thioredoxin inhibitor	0.587	0.032
	▪ TNF expression inhibitor	0.536	0.022
	▪ Fatty-acyl-CoA synthase inhibitor	0.544	0.037
	▪ CYP2A2 substrate	0.482	0.029
	▪ Anticonvulsant	0.490	0.038
	▪ Analgesic	0.449	0.053

3.1 Biological activity predictions

For the biological activity spectrum of the known phytoconstituent named Zerumbone, an online PASS result was produced. Zerumbone was chosen for its pharmacological

Table.2 Binding affinities of isolated compound Zerumbone and standard at the active site of Secretory Phospholipase A2 (4UY1), Cyclooxygenase-2 (5IKT), Tumor Necrosis Factor (2AZ5), Inducible Nitric Oxide Synthase (4NOS)

Ligands	Proteins	Highest to the lowest mode of conformation with corresponding RMS binding affinities in ΔG (Kcal/mol)				
Zerumbone	4UY1	-7.4	-7.1	-6.1	-5.5	-5.1
	5IKT	-7.3	-7.0	-6.9	-6.6	-6.0
	2AZ5	-7.2	-7.1	-6.6	-5.2	-4.2
	4NOS	-6.5	-6.4	-6.3	-6.2	-5.5
5-(2,5-dimethyl-3-thienyl)-1h-pyrazole-3-carboxamide	4UY1	-7.2	-6.9	-6.7	-6.4	-5.9

Table.3 Interaction of ligands with amino acids residue at receptor site

Ligands	Cavity Size	Binding Affinity, ΔG (Kcal/mol)	Amino acids involved and Distance (A°)		
			Hydrogen binding interactions	Distance	H-Bond Type
Zerumbone+4uy1	687	-7.4	Ligand (O)---GLY28A (NH) Ligand (H)---CYS43A (SG)	3.18 2.68	Acceptor Donor
Zerumbone+5ikt	3546	-7.3	Ligand (H)---GLY225A(OH) Ligand (H)---ASN375A(OH)	2.69 2.58	Acceptor Acceptor
Zerumbone+2az5	233	-7.3	---	---	---
Zerumbone+4Nos	28146	-6.5	---	---	---
5-(2,5-dimethyl-3-thienyl)-1h-pyrazole-3-carboxamide+4uy1	687	-7.2	Ligand (N)---GLY28A (N) Ligand (H)---ASP47A (OD)	3.04 2.81	Acceptor Donor

activity based on its higher Pa value (Pa > 0.07). This prediction was interpreted and applied appropriately in table 1.

3.2 Molecular Docking Analysis

The docking score was employed in the current investigation to validate the probable binding affinity of drugs responsible for anti-inflammatory effects. The maximum binding affinity score in the PyRx system defines the optimal docking connection between protein and ligand, and the binding score of all phytochemicals is provided in Tables 2 and 3.

The protein-ligand docking data showed excellent docking with the targeted receptors, particularly Secretory Phospholipase A2. Zerumbone has the best docking score of -7.4 Kcal/mol with the Secretory Phospholipase A2 receptor. Aside from that, it demonstrated docking scores of -7.3, -7.2, and -6.5 Kcal/mol with the receptors Cyclooxygenase 2, Tumor Necrosis Factor, and Inducible Nitric Oxide Synthase 4, respectively. The co-crystallized ligand of the receptor Secretory Phospholipase A2, 5-(2,5-dimethyl-3-thienyl)-1h-pyrazole-3-carboxamide, which has been reported as a SPLA2 inhibitor, was docked with Secretory Phospholipase A2 separately to compare the binding affinity of Zerumbone with the co-crystallized ligand. The docking score of the co-crystallized native ligand, 5-(2,5-dimethyl-3-thienyl)-1h-pyrazole-3-carboxamide, with receptor Secretory Phospholipase A2 was-7.2 Kcal/mol, which was quite low in comparison to the binding affinity previously observed between the Zerumbone and Secretory Phospholipase A2 receptor. The interactions between the atoms of the specified ligands and the amino acid residues of the target proteins are depicted in Figures 3 and 4.

3.3 Molecular Dynamics Simulation of Protein-Ligand Complex

An effective technique for assessing the stability of protein-ligand complexes is molecular dynamics (MD) simulation. Only the best docking complex Zerumbone and Secretory Phospholipase A2 considered MD simulation. With the aid of RMSD (Root Mean Square Deviation), RMSF (Root Mean Square Fluctuation) and RG (Radius of gyration), MD trajectories analysis was carried out to assess the stability and fluctuations of this complex.

The compactness of the protein following the ligand-induced fit into it may be examined using the root-mean-square deviation (RMSD) [60, 61]. To calculate the RMSD, backbone atoms' atomic coordinates from their trajectories were acquired. It is determined by taking the RMS values of these atomic positions and routing them. Greater stability is shown by a decrease in the complex's RMSD values' volatility. Successful docking was designated by an RMSD value of fewer than 1.5 angstroms [62]. The secretory phospholipase A2 protein combination with Zrumbone is depicted in figure 5 as having RMSD values of less than 1.5, indicating that the complex did not exhibit any unfavorable repulsion and had good stability.
The root-mean-square fluctuation (RMSF) method may also be used to determine the conformational stability of a macromolecular system. It is calculated using the same method as the RMSD, except this time it focuses on the individual residue flexibility. Lower the fluctuation of coordinates indicates the greater the stability. The whole RMSF profile for each residue dynamics of the target receptor was presented, revealing consistent atomic-pattern variations at MDS. The peak fluctuation areas of 0.1-200 Å in figure 6 predicted that the ligand was binding at this location of the Secretory Phospholipase A2 receptor. Figure 6 shows that the amino acid residues Leu32, Glu62, Thr112, Val114, and Val125 fluctuated moderately but did not exceed RMSF <3.5 Å [63]. This indicates that the compound contains flexible residues with acceptable RMSF values.

The radius of gyration (Rg) is a metric used to calculate the strength of a macromolecular system using trajectories acquired from MD simulations. It is the distance between the center of mass and the axis of rotation [64]. Conformational stability in terms of Rg is defined as less fluctuation in Rg values indicating greater conformational stability of the protein-ligand system or

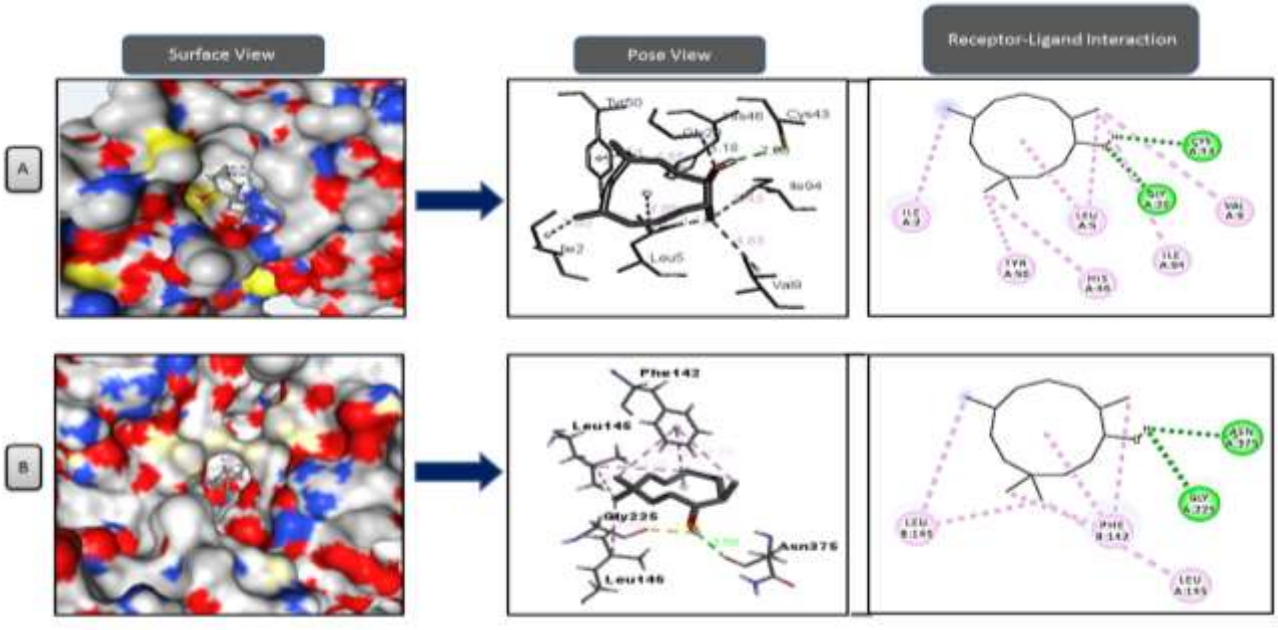

Figure 3. Possible 3D and 2D interactions of A) Zerumbone and Secretory Phopholipase A2. B) Zerumbone and Cyclooxygenase-2 receptor.

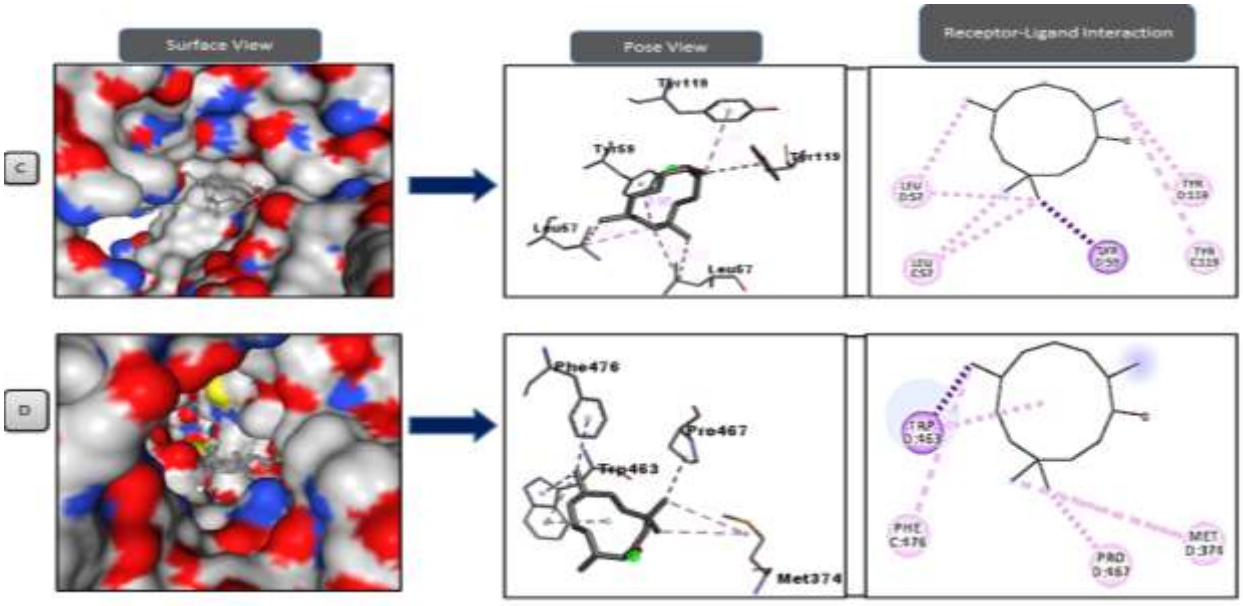

Figure 4. Possible 3D and 2D interactions of A) Zerumbone and Tumor Necrosis Factor. B) Zerumbone and Inducible Nitric Oxide Synthase 4 receptor.

complex [65]. Rg values less than the average suggest a more compact system [66]. Figure 7 can be used to analyze the complex's radius of gyration at 300k. Rg values were determined to be between 2.40 and 2.45 nm till the end. The complete investigation found that the trajectory had a peak value of ~2.55 nm in the early stages. Later, this high value was never seen over again, indicating protein stability in the complex and no dramatic structural changes in the protein.

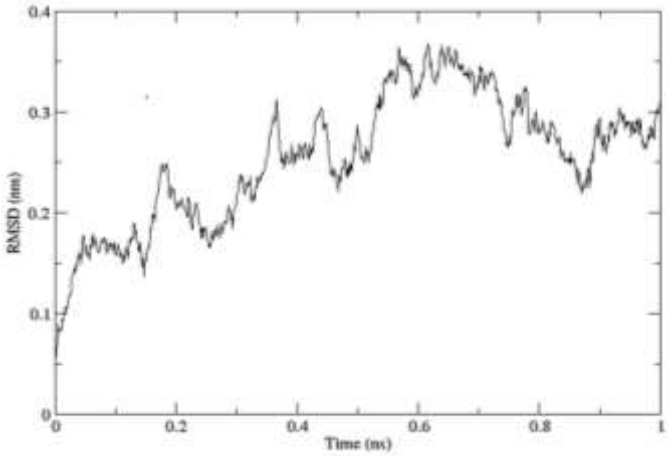

Figure 5. RMSD fits to backbone for the complex between Zerumbone and Secretory Phospholipase A2

Depending on the structural interactions between proteins and ligands, the IMOD server disclosed the internal coordinates analysis [10]. IMODs also calculate the B-factor and assess the structural deformation and eigenvalue.

The docked combination of our protein and ligand is shown in Image A of Figure 8. The deformability graph is shown in Image B of Figure 8. The deformity graph showed peaks in the graph that correspond to sections of the protein that are flexible. The eigenvalue of the complex is shown in image C of figure 8. The motion stiffness is represented by the eigenvalue connected to each normal mode. The energy needed to deform the structure has a direct impact on its value. The ease of deformation increases with decreasing eigenvalue. An eigenvalue of 5.580678e-05 was observed in our docked complex. The variance plot is shown in Image D of Figure 8. Individual variations are shown on the variance plot in the color red, while cumulative variance is shown in the color green. The elastic map of our docked complex is shown in Image E of Figure 8. One spring is represented by each dot in the graph for each atom pair. According to spring stiffness, the dots are colored differently; darker grey dots represent stiffer springs and vice versa.

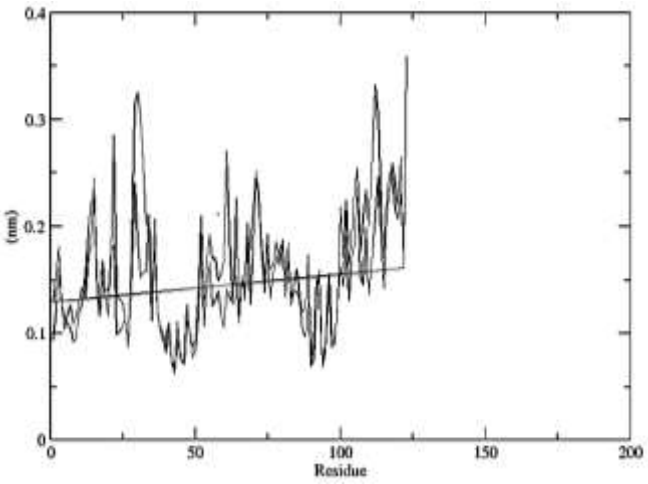

Figure 6. RMSF for the complex between Zerumbone and Secretory Phospholipase A2

The covariance map may be seen in Image F of Figure 8. The correlation motion between two residues is shown in red on this map, whereas the uncorrelated and anticorrelated motions are shown in white and blue, respectively. Figure 8's Image G is a representation of the B-Factor graph. A measurement of a particular molecule's capacity to deform at each of its residues is known as the main-chain deformability or B-Factor. Above such conditions, it was clear that our complex exhibited a significant degree of deformability. It also displayed a moderately low eigenvalue, indicating that it was easily deformable. The variance map showed that cumulative

variances were more significant than individual variances. The elastic network map also delivered successful attributes.

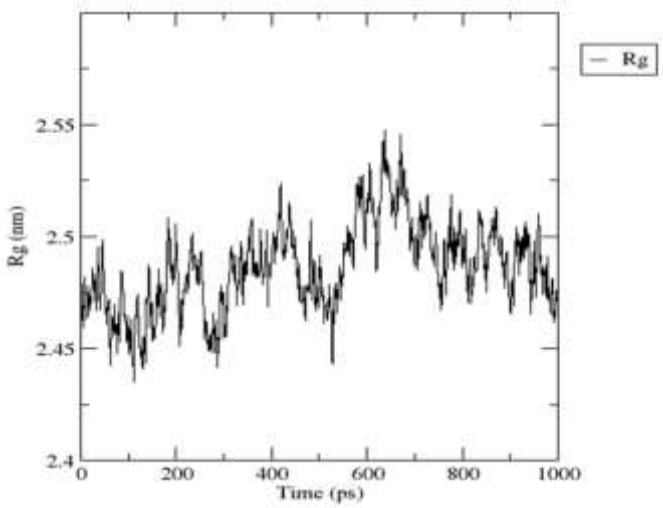

Figure 7. A) Radius of Gyration of Zerumbone and Secretory Phospholipase A2 complex, B) Hydrogen bonds of Zerumbone and Secretory Phospholipase A2 complex, C) Solvent accessible surface area study of Zerumbone and Secretory Phospholipase A2 complex

3.4 *In silico* pharmacokinetic and physicochemical properties *ADMET properties*

3.4.1 ADMET properties

To ascertain a compound's physicochemical interaction with a certain target, it is crucial to research diverse compounds' absorption, distribution, metabolism, excretion, and toxicity (ADMET). During the research and development of novel drugs, this enables us to assess their potential as drug candidates and, eventually, results in the identification of a new lead molecule for a particular target domain [67].

The goal of the current study is to identify the pharmacokinetic characteristics of chosen ligands to fully understand how they interact with the body. Human intestinal absorption (HIA) is a crucial rate-limiting stage in the delivery of a medicine to the target region where it will have pharmacological effects. It is challenging to predict HIA because of a variety of contributing variables. After being taken orally, medications are absorbed into the bloodstream and then transported through systemic circulation from the site of absorption to other organs. Drugs that are distributed to the target location have lower plasma concentrations. Enzymatic processes are used to break down certain medicines, and activated metabolites have pharmacological effects. On the other hand, inactive metabolites reduce the effects of the medication and are eliminated by the kidney.

According to the ADMET properties investigation (Table 4), Zerumbone has a blood-brain barrier (BBB) penetration rate of 5.00775 in vitro, indicating its better efficacy in distributing into the central nervous system. Furthermore, it demonstrated greater BBB penetration than standard 5-(2, 5-dimethyl-3-thienyl)-1h-pyrazole-3-carboxamide (0.390165). Zerumbone's in-vitro Caco-2 cell permeability was measured at 55.3568 nm/sec, whereas the standard 5-(2, 5-dimethyl-3-thienyl)-1h-pyrazole-3-carboxamide exhibited just 0.55911. That suggests Zerumbone is moderately permeable through Caco-2 cells to a significant extent. This Caco-2 cell permeability reveals that they are persistently permeable to PPB, allowing them to pass through the blood-brain barrier system. This conclusion is supported by the fact that the in-vitro plasma protein binding percentage of chosen ligand, which was seen in Zerumbone at 100%, demonstrated exceptionally high plasma protein binding affinity when compared to the 5-(2,5-dimethyl-3-thienyl)-1h-

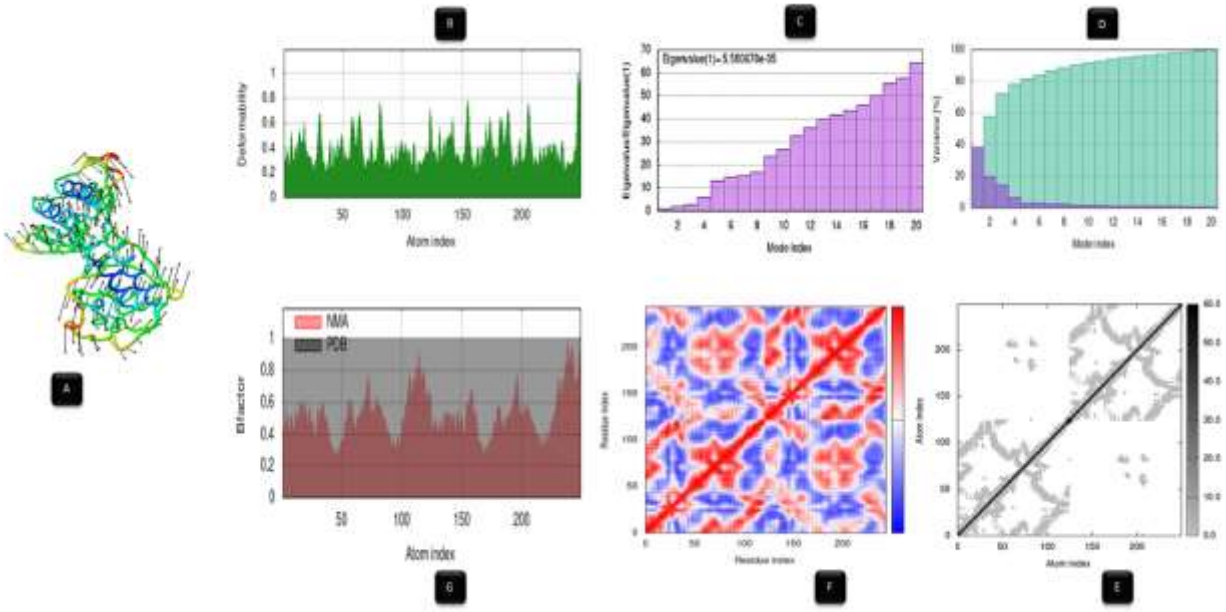

Figure 8. This figure shows results of Molecular Dynamics Simulations of the complex formed between our ligand and Secretory Phospholipase A2 receptor. Image A represents the docked complex of our protein and ligand. Image B represents the deformability graph. Image C represents the eigenvalue of the complex. Image D represents the variance plot. Image E represents the elastic map of our docked complex. Image F represents the covariance map. Image G represents

Table.4 ADMET properties of selective ligand and Standard

Name	BBB-penetration	Caco-2	PPB	MDCK	HIA	Skin permeability	Toxicity
Zerumbone	5.00775	55.3568	100	115.218	100	-0.641176	None
5-(2,5-dimethyl-3-thienyl)-1h-pyrazole-3-carboxamide	0.390165	0.55911	48.730	252.994	92.940		None

Table.5 Toxicity profile of selective ligand and Standard

Name	AMES Toxicity	Hepatotoxicity	Minnow Toxicity	hERG inhibition	Max. tolerated dose (human)
Zerumbone	No	No	No	No	0.534 log mg/kg/day
5-(2,5-dimethyl-3-thienyl)-1h-pyrazole-3-carboxamide	No	Yes	2.271 log mM	No	0.424 log mg/kg/day

Table.6 QSAR properties of selective ligand and Standard

Name	MW	logP	HBA	HBD	MR	TPSA	nRB	Violation
Zerumbone	218.17	4.143	1	0	72.49	17.07	0	0

Table.7 Bioactivity & toxicity risks of ligand and standard

Name	Structure	Bioactivity						Toxicity Risks	
		GPCRL	ICM	KI	NRL	PI	EI	Drug likeness	Score
Zerumbone	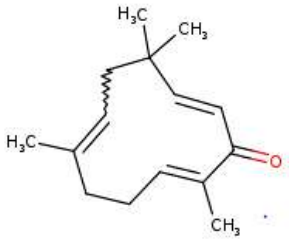	-0.28	-0.08	-1.07	0.22	-0.52	0.24	-1.97	0.38
5-(2,5-dimethyl-3-thienyl)-1h-pyrazole-3-carboxamide	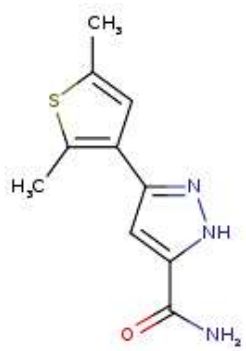	-0.84	-0.80	-0.13	-1.01	-0.94	-0.58	4.06	0.91

pyrazole-3-carboxamide with 48.730. Zerumbone and 5-(2,5-dimethyl-3-thienyl)-1h-pyrazole-3-carboxamide both had in-vitro Madin-Darby-Canine Kidney (MDCK) cell permeability values of 115.218 nm/sec and 252.994, respectively, indicating that they were both reasonably permeable compounds. Human intestinal absorption (HIA) as a percentage was determined to be 100, which is significantly greater than the standard (92.940). Skin permeability values of -0.641176 and -4.2498 for our selected ligand and standard were both negative. The toxicity result was likewise determined to be negative, which suggested that the ligands are secure and non-toxic. Finally, this ADMET examination of Zerumbone's characteristics indicated the

Figure 9. In the BOILED-EGG Model, the white part represents the physicochemical space of molecules most likely to be absorbed by the GI (gastrointestinal tract), while the yellow part represents molecules most likely to reach the brain.

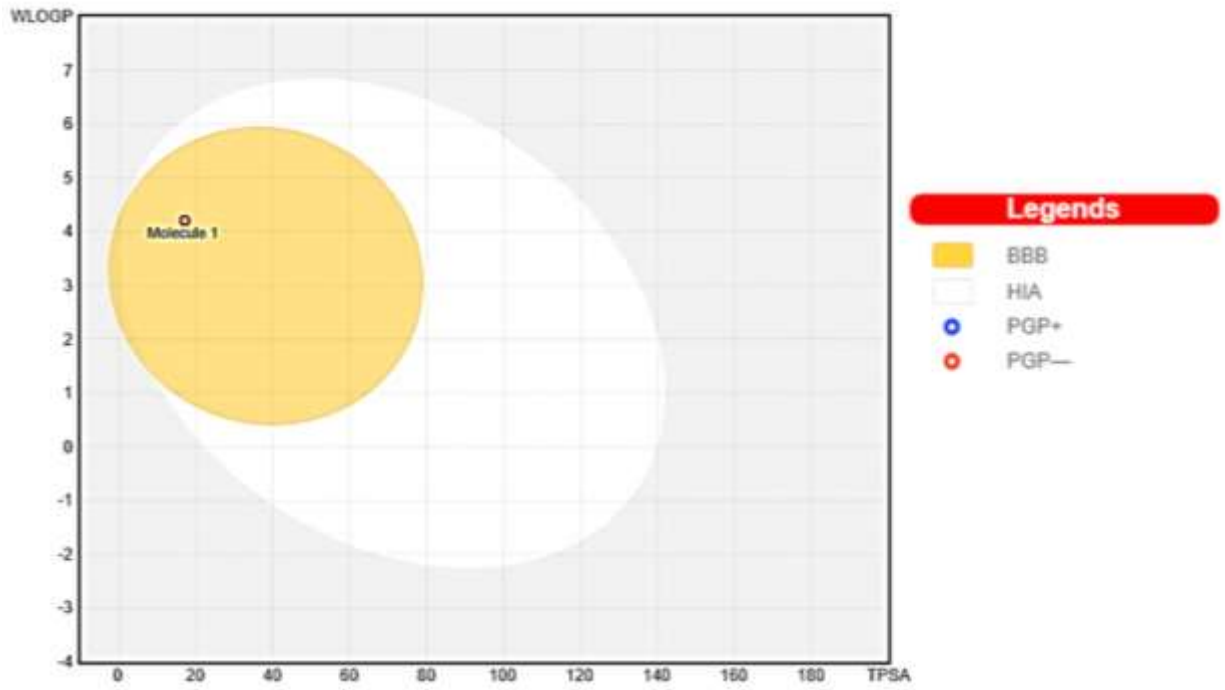

substance's excellent physic-chemical interaction and drug-like activity.

From the pkCSM-pharmacokinetics web-based server, the toxicity characteristics were further retrieved (Table 5). This server displayed the least toxicity indicators and human maximum tolerated dosage at 0.534 log mg/kg/day.

3.4.2 QSAR properties

An important step in evaluating a compound's drug-like qualities is to study its physicochemical interaction with the target domain. The chosen compound's potential biological interaction characteristics are predicted by the QSAR analysis. This study used the Lipinski rule of five to evaluate the selected ligands for some QSAR characteristics (Table 6). According to reports, the ligand Zerumbone has a molecular weight of 218.17 Da. As per the Lipinski first rule for efficient and safe drug delivery, this value was less than 500 Da. Another restriction is the presence of no more than five hydrogen bond donor groups. This rule was accepted by the ligand. The measured logP value was 4.14, which was no more than 5, and the number of hydrogen bond acceptor groups was 1, which was no more than 10. Additionally, a molecular refractivity calculation of 72.49 cm3/mol indicated a higher potential for a therapeutic candidate. Zerumbone had no Lipinski violations found. Additionally, the TPSA (total polar surface area) for Zerumbone was determined to be 17.07, which was not higher than 140. Finally, the predicted QSAR features of the selected ligand confirmed its efficient physicochemical interaction to exert and support powerful ligand qualities as an anti-inflammatory drug.

3.4.3 Boiled egg analysis

According to the Boiled-Egg plot, the Zerumbone exhibits an excessive level of blood-brain barrier permeability. Additionally, it was discovered that our drug molecule also had gastrointestinal retention properties (Figure 9).

3.4.4 Bioactivity and toxicity risk studies

Table 7 summarizes the bioactivity and toxicity risk profiles of selected ligands. We found the GPCRL property to be -0.28, ICM property to be -0.08, KI property to be -1.07, NRL interaction property to be 0.22, PI property to be -0.52, and EI property to be 0.24. KI and EI properties were both lower than the standard 5-(2, 5-dimethyl-3-thienyl)-1h-pyrazole-3-carboxamide. Additionally, the ligand showed -1.97 drug-likeness, which was lower than the standard (4.06). Also, the drug score of the ligand was estimated at 0.38, which was similar to the drug score of the standard (0.91). Based on the results of this bioactivity and toxicity analysis, it can be concluded that the ligands are safe as drug candidates as well as potentially bioactive against reactive species.

4. Conclusion

The study conducted on Zerumbone revealed that it could help decrease the inflammation levels in the body. Use of Zerumbone against inflammatory mediate receptors (Secretory Phospholipase A2, Cyclooxygenase-2, Tumor Necrosis Factor, and Inducible Nitric Oxide Synthase 4) is that the creation of an anti-inflammatory drug could be acceptable. The optimal binding affinities of Zerumbone against its targeted receptor were determined by the in-silico method. The Zerumbone had the highest docking score of -7.4 kcal/mol against Secretory Phospholipase A2, which was also revealed to be much greater than the binding affinity displayed by the native ligand when it was co-crystallized with the receptor. Additionally, our compound's QSAR, ADMET, Bioactivity, and Toxicity Score analyses came back with very promising results. Besides that, the MD simulation investigation of the docked complex of our ligand with Secretory Phospholipase A2 receptor demonstrated

excellent stability. Thus, it may be said that Zerumbone can provide treatment for inflammatory illnesses. Finally, In-vivo and in-silico investigations on our chemical might be encouraged us to determine its efficacy as well as to suggest the precise method for treating inflammatory illnesses.

Conflicting Interests

The authors have declared that no conflicting interests exist.

Authors' contributions

We confirm that the manuscript has been read and approved by all named authors. We further confirm that the order of authors listed in the manuscript has been approved by all of us. The contribution of all authors is equally evaluated. We understand that the Corresponding Author is the sole contact for the Editorial process (including Editorial Manager and direct communications with the office). He is responsible for communicating with the other authors about progress, submissions of revisions and final approval of proofs. We confirm that we have provided a current, correct email address which is accessible by the Corresponding Author.

References

1. Harvey, A., *Strategies for discovering drugs from previously unexplored natural products.* Drug discovery today, 2000. **5**(7): p. 294-300.
2. Bakhotmah, B.A. and H.A. Alzahrani, *Self-reported use of complementary and alternative medicine (CAM) products in topical treatment of diabetic foot disorders by diabetic patients in Jeddah, Western Saudi Arabia.* BMC Research Notes, 2010. **3**(1): p. 1-8.
3. Yadav, R. and M. Agarwala, *Phytochemical analysis of some medicinal plants.* Journal of phytology, 2011. **3**(12).
4. Arunkumar, S. and M. Muthuselvam, *Analysis of phytochemical constituents and antimicrobial activities of Aloe vera L. against clinical pathogens.* World journal of agricultural sciences, 2009. **5**(5): p. 572-576.
5. Dewick, P., *Tumor inhibition from plants.* Tease and Evans, 1996: p. 210-214.
6. Phillipson, J.D., et al., *Plants with antiprotozoal activity.* Trease and Evans' Pharmacognosy, 1996.
7. Bellik, Y., et al., *Phytochemicals to prevent inflammation and allergy.* Recent Patents on Inflammation & Allergy Drug Discovery, 2012. **6**(2): p. 147-158.
8. Hotamisligil, G.S., *Inflammation and metabolic disorders.* Nature, 2006. **444**(7121): p. 860-867.
9. Chen, H., et al., *Discovery of a novel pyrazole series of group X secreted phospholipase A2 inhibitor (sPLA2X) via fragment based virtual screening.* Bioorganic & Medicinal Chemistry Letters, 2014. **24**(22): p. 5251-5255.
10. Sengupta, S., et al., *In-Silico Modelling of 1-3-[3-(Substituted Phenyl) Prop-2-Enoyl) Phenyl Thiourea Against Anti-Inflammatory Drug Targets.* Biosciences Biotechnology Research Asia, 2021. **18**(2): p. 413.
11. Boyanovsky, B.B. and N.R. Webb, *Biology of Secretory Phospholipase A2.* Cardiovascular Drugs and Therapy, 2008. **23**(1).
12. Triggiani, M., et al., *Secretory phospholipases A2 in inflammatory and allergic diseases: not just enzymes.* Journal of Allergy and Clinical Immunology, 2005. **116**(5): p. 1000-1006.
13. Dennis, E.A. and P.C. Norris, *Eicosanoid storm in infection and inflammation.* Nature Reviews Immunology, 2015. **15**(8): p. 511-523.
14. Sanak, M., *Eicosanoid mediators in the airway inflammation of asthmatic patients: what is new?* Allergy, asthma & immunology research, 2016. **8**(6): p. 481-490.
15. Simmons, D.L., R.M. Botting, and T. Hla, *Cyclooxygenase isozymes: the biology of prostaglandin synthesis and inhibition.* Pharmacological reviews, 2004. **56**(3): p. 387-437.
16. Bindra, J., *Prostaglandin synthesis*. 2012: Elsevier.
17. Williams, T. and J. Morley, *Prostaglandins as potentiators of increased vascular permeability in inflammation.* Nature, 1973. **246**(5430): p. 215-217.
18. Yao, C. and S. Narumiya, *Prostaglandin-cytokine crosstalk in chronic inflammation.* British journal of pharmacology, 2019. **176**(3): p. 337-354.
19. Gunalan, G., et al., *Anti-inflammatory activities of phytochemicals from Bauhinia variegata Linn. leaf: An in silico approach.* J. chem. pharm, 2014. **6**(9): p. 334-48.
20. Gunalan, G., C. Romeo, and P. Sumathi, *Docking Studies of Pyrazole Derivative as Anti-Inflammatory Drug With Cyclooxgenase-2.* IJBST, 2011. **4**(12): p. 82-86.
21. Fu, J.-Y., et al., *The induction and suppression of prostaglandin H2 synthase (cyclooxygenase) in human monocytes.* Journal of Biological Chemistry, 1990. **265**(28): p. 16737-16740.
22. Crofford, L.J., et al., *Cyclooxygenase-1 and-2 expression in rheumatoid synovial tissues. Effects of interleukin-1 beta, phorbol ester, and corticosteroids.* The Journal of clinical investigation, 1994. **93**(3): p. 1095-1101.
23. Chu, W.-M., *Tumor necrosis factor.* Cancer Letters, 2013. **328**(2): p. 222-225.
24. Fischer, R. and O. Maier, *Interrelation of oxidative stress and inflammation in neurodegenerative disease: role of TNF.* Oxidative medicine and cellular longevity, 2015. **2015**.
25. Annibaldi, A. and P. Meier, *Checkpoints in TNF-induced cell death: implications in inflammation and cancer.* Trends in molecular medicine, 2018. **24**(1): p. 49-65.
26. Knowles, R.G. and S. Moncada, *Nitric oxide synthases in mammals.* Biochemical Journal, 1994. **298**(Pt 2): p. 249.
27. Jayashankar, B., et al., *Supercritical extract of Seabuckthorn leaves (SCE200ET) inhibited endotoxemia by reducing inflammatory cytokines and nitric oxide synthase 2 expression.* International Immunopharmacology, 2014. **20**(1): p. 89-94.
28. Korhonen, R., et al., *Nitric oxide production and signaling in inflammation.* Current Drug Targets-Inflammation & Allergy, 2005. **4**(4): p. 471-479.
29. Kröncke, K., K. Fehsel, and V. Kolb-Bachofen, *Inducible nitric oxide synthase in human diseases.* Clinical & experimental immunology, 1998. **113**(2): p. 147-156.
30. Cragg, G.M., D.J. Newman, and K.M. Snader, *Natural products in drug discovery and development.* Journal of natural products, 1997. **60**(1): p. 52-60.
31. Kim, Y.S., et al., *Bioactive Food Components, Inflammatory Targets, and Cancer PreventionDiet, Inflammation, and Cancer Prevention.* Cancer prevention research, 2009. **2**(3): p. 200-208.
32. Gautam, R. and S.M. Jachak, *Recent developments in anti-inflammatory natural products.* Medicinal research reviews, 2009. **29**(5): p. 767-820.
33. Calixto, J.B., M.F. Otuki, and A.R. Santos, *Anti-inflammatory compounds of plant origin. Part I. Action on arachidonic acid pathway, nitric oxide and nuclear factor κ B (NF-κB).* Planta medica, 2003. **69**(11): p. 973-983.
34. Al-Amin, M., et al., *Antimicrobial activity of the crude extract, fractions and isolation of zerumbone from the rhizomes of Zingiber roseum.* Journal of Research in Pharmacy, 2019. **23**(3): p. 559-566.
35. Kalantari, K., et al., *A Review of the Biomedical Applications of Zerumbone and the Techniques for Its Extraction from Ginger Rhizomes.* Molecules, 2017. **22**(10): p. 1645.

36. Al-Amin, M., G.N.N. Sultana, and C.F. Hossain, *Antiulcer principle from Zingiber montanum.* Journal of Ethnopharmacology, 2012. **141**(1): p. 57-60.
37. Sulaiman, M., et al., *Preliminary analysis of the antinociceptive activity of zerumbone.* Fitoterapia, 2009. **80**(4): p. 230-232.
38. Sulaiman, M., et al., *Anti-inflammatory effect of zerumbone on acute and chronic inflammation models in mice.* Fitoterapia, 2010. **81**(7): p. 855-858.
39. Sulaiman, M.R., et al., *Anti-inflammatory effect of zerumbone on acute and chronic inflammation models in mice.* Fitoterapia, 2010. **81**(7): p. 855-858.
40. Somchit, M., et al., *Zerumbone isolated from Zingiber zerumbet inhibits inflammation and pain in rats.* Journal of Medicinal Plants Research, 2012. **6**(2): p. 177-180.
41. Goel, R.K., et al., *PASS-assisted exploration of new therapeutic potential of natural products.* Medicinal Chemistry Research, 2011. **20**(9): p. 1509-1514.
42. Khurana, N., et al., *PASS assisted prediction and pharmacological evaluation of novel nicotinic analogs for nootropic activity in mice.* European journal of pharmacology, 2011. **662**(1-3): p. 22-30.
43. Mittal, M., et al., *PASS-assisted exploration of antidepressant activity of 1, 3, 4-trisubstituted-β-lactam derivatives.* Bioorganic & medicinal chemistry letters, 2008. **18**(20): p. 5347-5349.
44. Amanat, M., et al., *Zingiber roseum Rosc. rhizome: A rich source of hepatoprotective polyphenols.* Biomedicine & Pharmacotherapy, 2021. **139**: p. 111673.
45. Yang, Z., et al., *UCSF Chimera, MODELLER, and IMP: an integrated modeling system.* Journal of structural biology, 2012. **179**(3): p. 269-278.
46. Berman, H.M., et al., *The Protein Data Bank archive as an open data resource.* Journal of computer-aided molecular design, 2014. **28**(10): p. 1009-1014.
47. Kalimuthu, A.K., et al., *Pharmacoinformatics-based investigation of bioactive compounds of Rasam (South Indian recipe) against human cancer.* Scientific Reports, 2021. **11**(1).
48. Dey, D., et al., *Molecular optimization, docking, and dynamic simulation profiling of selective aromatic phytochemical ligands in blocking the SARS-CoV-2 S protein attachment to ACE2 receptor: an in silico approach of targeted drug designing.* Journal of Advanced Veterinary and Animal Research, 2021. **8**(1): p. 1.
49. simulation, W.f.m. *Simlab*. 21.06.2022]; Available from: https://simlab.uams.edu/.
50. Kuriata, A., et al., *CABS-flex 2.0: a web server for fast simulations of flexibility of protein structures.* Nucleic acids research, 2018. **46**(W1): p. W338-W343.
51. Schüttelkopf, A.W. and D.M. Van Aalten, *PRODRG: a tool for high-throughput crystallography of protein–ligand complexes.* Acta Crystallographica Section D: Biological Crystallography, 2004. **60**(8): p. 1355-1363.
52. Berendsen, H., J. Grigera, and T. Straatsma, *The missing term in effective pair potentials.* Journal of Physical Chemistry, 1987. **91**(24): p. 6269-6271.
53. Jamroz, M., A. Kolinski, and S. Kmiecik, *CABS-flex predictions of protein flexibility compared with NMR ensembles.* Bioinformatics, 2014. **30**(15): p. 2150-2154.
54. pkCSM. *Pharmacokinetic properties* 20.06.2022]; Available from: http://biosig.unimelb.edu.au/pkcsm/prediction.
55. Organic Chemistry Portal. *Molecular Property Explorer*. 21.06.2022]; Available from: https://www.organic-chemistry.org/prog/.
56. Swiss Institute of Bio-informatics. *SwissADME*. 20.06.2022]; Available from: http://www.swissadme.ch/index.php.
57. Wang, Y., et al., *In silico prediction of human intravenous pharmacokinetic parameters with improved accuracy.* Journal of chemical information and modeling, 2019. **59**(9): p. 3968-3980.
58. Islam, M.A. and T.S. Pillay, *Identification of promising anti-DNA gyrase antibacterial compounds using de novo design, molecular docking and molecular dynamics studies.* Journal of Biomolecular Structure and Dynamics, 2020. **38**(6): p. 1798-1809.
59. Daina, A., O. Michielin, and V. Zoete, *SwissADME: a free web tool to evaluate pharmacokinetics, drug-likeness and medicinal chemistry friendliness of small molecules.* Scientific reports, 2017. **7**(1): p. 1-13.
60. Lindorff-Larsen, K., et al., *Improved side-chain torsion potentials for the Amber ff99SB protein force field.* Proteins: Structure, Function, and Bioinformatics, 2010. **78**(8): p. 1950-1958.
61. Abraham, M.J., et al., *GROMACS: High performance molecular simulations through multi-level parallelism from laptops to supercomputers.* SoftwareX, 2015. **1**: p. 19-25.
62. Kumar, D., et al., *Promising inhibitors of main protease of novel corona virus to prevent the spread of COVID-19 using docking and molecular dynamics simulation.* Journal of Biomolecular Structure and Dynamics, 2020. **39**(13): p. 4671-4685.
63. Tumskiy, R.S. and A.V. Tumskaia, *Multistep rational molecular design and combined docking for discovery of novel classes of inhibitors of SARS-CoV-2 main protease 3CLpro.* Chemical Physics Letters, 2021. **780**: p. 138894.
64. Rahman, M.M., et al., *Virtual screening, molecular dynamics and structure–activity relationship studies to identify potent approved drugs for Covid-19 treatment.* Journal of Biomolecular Structure and Dynamics, 2021. **39**(16): p. 6231-6241.
65. Kumar, B., et al., *In silico screening of therapeutic potentials from Strychnos nux-vomica against the dimeric main protease (Mpro) structure of SARS-CoV-2.* Journal of Biomolecular Structure and Dynamics, 2021: p. 1-19.
66. Gupta, S., et al., *Identification of potential natural inhibitors of SARS-CoV2 main protease by molecular docking and simulation studies.* Journal of Biomolecular Structure and Dynamics, 2021. **39**(12): p. 4334-4345.
67. Oprea, T.I. and H. Matter, *Integrating virtual screening in lead discovery.* Current opinion in chemical biology, 2004. **8**(4): p. 349-358.

.